

Ultrafast Mott transition driven by nonlinear electron-phonon interaction

Francesco Grandi,¹ Jiajun Li,¹ and Martin Eckstein¹

¹*Department of Physics, University of Erlangen-Nürnberg, 91058 Erlangen, Germany*

(Dated: January 27, 2021)

Nonlinear phononics holds the promise for controlling properties of quantum materials on the ultrashort timescale. Using nonequilibrium dynamical mean-field theory, we solve a model for the description of organic solids, where correlated electrons couple non-linearly to a quantum phonon-mode. Unlike previous works, we exactly diagonalize the local phonon mode within the non-crossing approximation (NCA) to include the full phononic fluctuations. By exciting the local phonon in a broad range of frequencies near resonance with an ultrashort pulse, we show it is possible to induce a Mott insulator-to-metal phase transition. Conventional semiclassical and mean-field calculations, where the electron-phonon interaction decouples, underestimate the onset of the quasiparticle peak. This fact, together with the non-thermal character of the photo-induced metal, suggests a leading role of the phononic fluctuations and of the dynamic nature of the state in the vibrationally induced quasiparticle coherence.

Introduction - In the last decade, nonlinear phononics [1, 2] has become one of the most promising pathways for the non-equilibrium control of quantum materials [3]. Within this approach, one can transiently stabilize a crystal structure unstable under equilibrium conditions by coherently exciting an infrared-active lattice mode which is nonlinearly coupled to a Raman-active phonon [4–10]. An analogous pathway suggests that the electronic properties of solids may be manipulated by the excitation of vibrational modes that couple non-linearly with the local degrees of freedom of the electronic system [11–16].

Molecular solids provide a perfect playground for testing this mechanism [17, 18]. A paradigm example is the charge transfer salt ET-F₂TCNQ, which is an archetypical one-dimensional Mott insulator under equilibrium conditions and has been widely studied under photo-doping [19, 20]. Upon excitation of the molecular vibration $\omega_{\text{ph}} = 1000 \text{ cm}^{-1}$, the charge transfer (CT) resonance at $\sim 5500 \text{ cm}^{-1}$ is red-shifted, and an in-gap state at $2 \times \hbar\omega_{\text{ph}}$ appears [11, 21]. Even more intriguing results have been obtained regarding light-induced superconductivity. The fulleride K₃C₆₀ [22] shows a superconducting state at temperatures almost ten-times higher than the equilibrium T_c lasting few-picoseconds after excitation in the frequency range related to the T_{1u} mode of the C₆₀ molecule [23–25]. The organic superconductor $\kappa - (\text{BEDT} - \text{TTF})_2 \text{Cu} [\text{N} (\text{CN})_2] \text{Br}$ (henceforth $\kappa - \text{Br}$) displays a similar behavior when the C=C stretching mode of the $(\text{BEDT} - \text{TTF})^{+0.5}$ molecule is excited [26]. Because the photo-induced superconducting response is correlated with the presence of an equilibrium coherent quasiparticle, it is an obvious relevant question, which will be analyzed in this paper, whether non-linear phononics can enhance quasiparticle coherence in correlated electron systems. Moreover, we might ask if it is possible at all to replace the non-linear phonons with some time-dependent electronic Hamiltonian parameter. The rationale beyond this idea comes from a “natural” decoupling of the electron-phonon interaction. A typical local electron-phonon interaction gO_iX_i , where an electronic operator O_i couples to the displacement X_i of

atom i , would give a term $F_i(t)O_i$ with a time-dependent “force” $F_i(t) = g\langle X_i(t) \rangle$ in the electronic Hamiltonian when X_i is replaced by its time-dependent expectation value in a coherent (macroscopically occupied) $\mathbf{q} = 0$ phonon state. For example, the experiments on ET-F₂TCNQ and $\kappa - \text{Br}$ were interpreted by an average shift and a periodic time-dependence of the local Coulomb interaction (the Hubbard U) [11, 26, 27]. However, it is clear that the approximation $O_iX_i \approx O_i\langle X_i(t) \rangle$ is controlled by the fluctuations of the local displacement operator X_i relative to $\langle X_i(t) \rangle$, which are significant even when the phonons are globally in a macroscopic coherent mode. Even though the decoupling approach can successfully capture some experimental observations, it is, therefore, important to understand how quantum effects become manifest in nonlinear electron-phononics [21].

In this paper, we study a generalization of the Hubbard-Holstein model [28, 29], which applies to ET-F₂TCNQ and $\kappa - \text{Br}$, with a quadratic coupling of a local displacement X_i to the doublon and the holon densities, so that, on average, X_i^2 modulates a local electron interaction U . The simulations indeed predict an insulator-to-metal transition (IMT), with a strong enhancement of the quasiparticle weight driven by the excitation of the local vibration. The vibrationally induced metallicity in the model cannot be accounted for by a decoupled Hamiltonian in which a time-dependent U replaces the effect of the phonons, but instead the full quantum dynamics must be taken into account. We show that, even if the decoupled model takes into account the back-action of the electrons on the phonons (and vice versa), it cannot capture phonon-related features in the electronic spectrum (Fano resonances) [30, 31].

Model - We consider the generalized Hubbard-Holstein model, compactly written as:

$$H(t) = H_{\text{el}} + H_{\text{el-ph}} + H_{\text{ph}} + H_{\text{driv}}(t) - \mu N. \quad (1)$$

The purely electronic part of the Hamiltonian is given by

$$H_{\text{el}} = -v_0 \sum_{\langle i,j \rangle, \sigma} \left(c_{i,\sigma}^\dagger c_{j,\sigma} + \text{H. c.} \right) + U \sum_i n_{i,\uparrow} n_{i,\downarrow}, \quad (2)$$

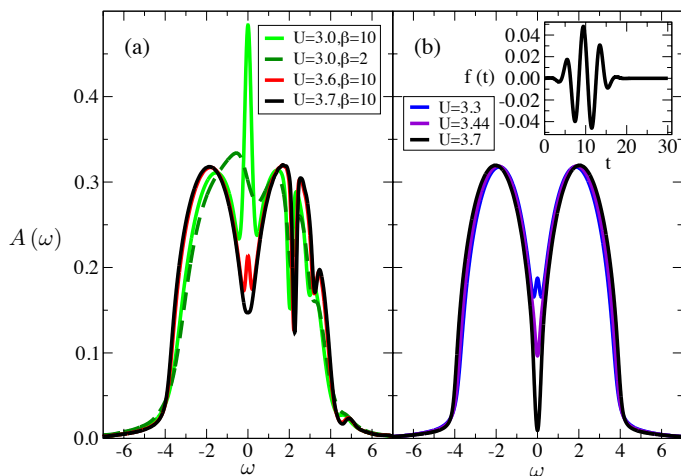


Figure 1. (Color online) (a) Equilibrium spectral functions $A(\omega)$ for the electron-phonon coupled system at several values of U and inverse temperature β . (b) Same for the Hubbard model without dynamic phonons, at $\beta = 10$. Inset: time dependent driving field $f(t)$, cf. Eq. (4). We keep the maximum amplitude (0.05) and the duration (20), while the frequency Ω is changed ($\Omega = 1.5$ in the plot, equal to ω_{ph}).

with nearest-neighbor hopping v_0 and local Hubbard interaction U ; μ is the chemical potential used to fix the occupation of each site to $\langle n_i \rangle = 1$. $v_0 = 1$ and \hbar/v_0 set the units for the energy and the times, respectively. The bare phonon Hamiltonian in Eq. (1) describes a band of Einstein phonons $H_{\text{ph}} = \omega_{\text{ph}} \sum_i (a_i^\dagger a_i + \frac{1}{2})$ where a_i^\dagger (a_i) are the creation (destruction) operator for a boson.

The electron-phonon interaction is given by [21]:

$$H_{\text{el-ph}} = 2 \sum_i (hH_i - dD_i) X_i^2, \quad (3)$$

where $H_i = (1 - n_{i,\uparrow})(1 - n_{i,\downarrow})$ ($D_i = n_{i,\uparrow}n_{i,\downarrow}$) are the holon (doublon) operators, and $X_i = \frac{a_i^\dagger + a_i}{\sqrt{2}}$ is the local displacement.

We take parameters $\omega_{\text{ph}} = 1.5$, so that we are far from the adiabatic regime, and assume the values $h = 0.1$ and $d = 0.35$ for the coupling constants. With this, the renormalized phonon frequencies on an isolated site occupied by a holon or doublon are $\omega_{\text{ph}}^h \sim 1.24 \omega_{\text{ph}}$ and $\omega_{\text{ph}}^d \sim 0.26 \omega_{\text{ph}}$, respectively. The renormalized frequency values obtained this way are in qualitative agreement with what found for ET-F₂TCNQ, where a stiffening of the holon oscillator and a slackening of the doublon one is observed [21]. Note that $H_{\text{el-ph}}$ with $d \neq h$ breaks the particle-hole symmetry even on a bipartite lattice [32]. In experiments, the quadratic coupling of the phonon-displacement and the electrons is confirmed by the $2\omega_{\text{ph}}$ feature in the optical absorption after phonon excitation [21]. The last term in Eq. (1) describes a linear coupling of the phonon displacement to an external

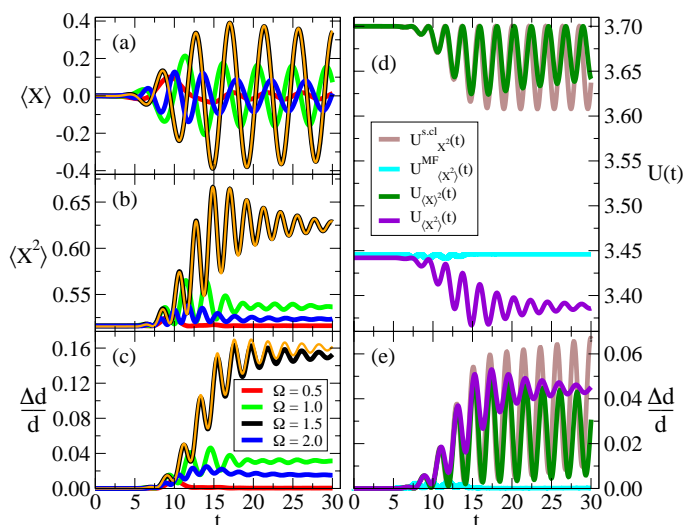


Figure 2. (Color online) Time evolution of the expectation value of the position operator $\langle X \rangle$ (a), its square $\langle X^2 \rangle$ (b), the relative change of the double occupations with respect to the initial value $\frac{\Delta d}{d} = \frac{d(t) - d(0)}{d(0)}$ (c), at $U = 3.7$, $\beta = 10$, and field pulses $f(t)$ of different frequencies Ω . The thin orange lines represent the results at $\Omega = 1.5$ without Ohmic bath. (d) Time dependent $U_{X^2}^{\text{sc}}(t)$, $U_{(X^2)}^{\text{MF}}(t)$, $U_{(X^2)}(t)$, and $U_{(X^2)}(t)$, as defined in Eq. (6). For the protocols $U_{(X^2)}(t)$, and $U_{(X^2)}(t)$ the expectation value $\langle X(t) \rangle$ and $\langle X^2(t) \rangle$ correspond to the black line at $\Omega = 1.5$ of panels a and b. (e) Time-dependent $\frac{\Delta d}{d}$ as obtained from Eq. (5), with $U(t)$ shown in panel d.

electric field,

$$H_{\text{driv}}(t) = \sqrt{2}\omega_{\text{ph}}f(t) \sum_i X_i, \quad (4)$$

and we use a few-cycle excitation pulse $f(t)$ with different frequencies Ω (see Fig. 1 inset) to excite a coherent vibration of the phonon. Finally, we will compare the dynamics obtained from Eq. (1) with a decoupled Hamiltonian, in which the electron dynamics is determined by Eq. (2) with a time-dependent interaction U

$$H_{U\text{-driv}}(t) = H_{\text{el}}[U \rightarrow U(t)], \quad (5)$$

with different forms of $U(t)$ as described in the text.

We solve the time-dependent models Eq. (1) and Eq. (5) using non-equilibrium dynamical mean-field theory (NEDMFT) within non-crossing approximation (NCA) [33, 34]. NCA has limitations in the description of the metallic phase of the Hubbard model at low temperatures and small U . Here, we apply it at high temperature and intermediate values of U ($U \sim$ bandwidth), where it is known to be qualitatively correct. NEDMFT maps the lattice problem into an Anderson impurity model with a self-consistent hybridization function $\Delta(t, t')$. We use a semi-elliptic free density of states of width $4v_0$, leading to the closed form $\Delta(t, t') = v_0^2 G(t, t')$ in terms of the local contour-ordered

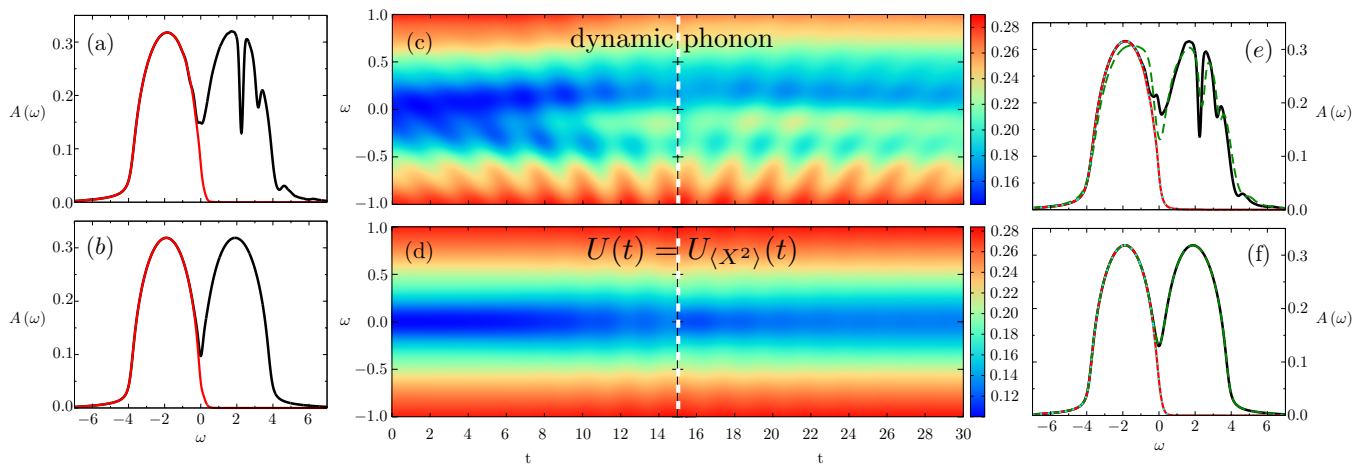


Figure 3. (Color online) Spectral functions for the dynamic phonon model at $U = 3.7$ (upper row) and the simplified approach $U(t) = U_{\langle X^2 \rangle}(t)$ (bottom row). Spectral function and occupation (black and red lines, respectively) at initial time $t = 0$ and at latest time $t = 30$ are shown in the left (a-b) and right columns (e-f), respectively. For intermediate time-steps see App. A. Additional lines in (e) and (f) show a fit $A^<(\omega, t) = A(\omega, t)/(1 + e^{\beta_{\text{eff}}\omega})$ to the occupation functions (dotted cyan lines), and the equilibrium spectral function (dashed green lines) for a systems with the same total energy as the driven system at latest time $t = 30$ ($\beta \sim 2.083$ for the phonon case, $U \sim 3.388$ and $\beta = 10$ for the U -driven case). Middle panels (c-d): Time dependent spectral weight close to the Fermi level $\omega = 0$; spectral functions are obtained by forward Fourier transform $A(\omega, t) = -\frac{1}{\pi} \text{Im} \int ds G^R(t+s, t) e^{i\omega s}$ for $t < 15$ and by backward Fourier transform for $t > 15$ (dashed vertical line at $t = 15$).

electronic Green's function $G(t, t')$. For model (1), we include the full phonon Fock space and the nonlinear local electron-phonon dynamics exactly in the DMFT impurity model (similar to bosonic DMFT [35]) and take the cutoff in the phonon Hilbert space large enough ($N_{\text{ph}} = 18$ for mean occupations $|\langle X \rangle| \lesssim 1$). This avoids potential ambiguities of alternative diagrammatic approaches for the local electron-phonon interaction [36–38]. Finally, energy dissipation of electrons to other degrees of freedom (phonons, spin fluctuations, etc.), which is fast in correlated insulators, is taken into account through a bosonic heat bath. The bath just adds a term to the hybridization [39, 40], $\Delta(t, t') = v_0^2 G(t, t') + \Delta_{\text{Ohmic}}(t, t')$, where $\Delta_{\text{Ohmic}}(t, t') = \lambda G(t, t') D_{\text{Ohmic}}(t, t')$ is second-order in the electron-boson coupling with temperature $1/\beta$ and Ohmic density of states (bath spectral density $J(\omega) = \sum_{\alpha} g_{\alpha}^2 \delta(\omega - \omega_{\alpha}) = \omega \theta(\omega_c - \omega)$, $\omega_c = 0.2$). We take $\lambda = 0.242$, which is weak enough so that electronic spectra are not affected by the coupling to the bath.

Results - In Fig. 1a, we plot the electronic spectral function $A(\omega)$ of the model (1) for several values of the interaction U . At inverse temperature $\beta = 10$, shared by both the electronic and lattice subsystems, there is an IMT around $U = 3.6$, indicated by the appearance of a quasi-particle peak at $\omega \sim 0$. With increasing temperature, the quasi-particle peak vanishes, as the system crosses over into a bad metallic regime (see data for $U = 3.0$ and $\beta = 2$). The pronounced dip in the upper Hubbard band results from the hybridization between the doublon states and the phonon.

We now concentrate on parameters $U = 3.7$ and $\beta = 10$ above the IMT and attempt to induce the transition through phonon driving. The vibrational mode is

pumped using a few-cycle pulse $f(t)$ as shown in the inset of Fig. 1, at different frequencies Ω . Figure 2 displays the resulting time-evolution of several observables. While $\langle X \rangle$ oscillates around its equilibrium position $\langle X \rangle = 0$ with the bare phonon frequency $\sim \omega_{\text{ph}}$ (Fig. 2a), $\langle X^2 \rangle$ oscillates around a shifted mean at a frequency $\sim 2\omega_{\text{ph}}$ (Fig. 2b). The most pronounced response is observed at resonant pumping $\Omega = \omega_{\text{ph}} = 1.5$. At resonance, the double occupancy increases by about 15% compared to its initial value (Fig. 2c). These changes go along with a photo-induced metallicity, as observed from the transient appearance of a quasi-particle peak at $\omega \sim 0$ in the time-resolved spectral function (Fig. 3, upper panels). The metallization survives the switch-off of the laser pulse up to the latest time ($t = 30$) of the simulation (Fig. 3e). In addition to the quasi-particle peak, one observes oscillations at frequency $2\omega_{\text{ph}}$ in the spectrum, like in $\langle X^2 \rangle$. The broad range of frequencies Ω where we observe the onset of the peak at $\omega \sim 0$ verifies the genuine metallicity of the photo-induced state, with a small asymmetry around the observed maximum response, see Fig. 4.

We will now contrast these results with the decoupled model Eq. (5), where phonon variables in the electron-phonon interaction Eq. (3) are replaced by a classical field or the expectation value of a quantum operator, leading to a time-dependent interaction. We compare four possible ansatzes: (i) X_i^2 is replaced by a classical field $X(t)^2$ self-consistently determined by the semi-classical equation of motion, (ii) a mean-field decoupling of the electron-phonon interaction Eq. (3) (of the kind $O_i X_i^2 \rightarrow \langle O_i \rangle X_i^2 + \langle X_i^2 \rangle O_i - \langle O_i \rangle \langle X_i^2 \rangle$) is performed while the full quantum dynamics of phonons is considered with the equation of motion for the density matrix, and X^2

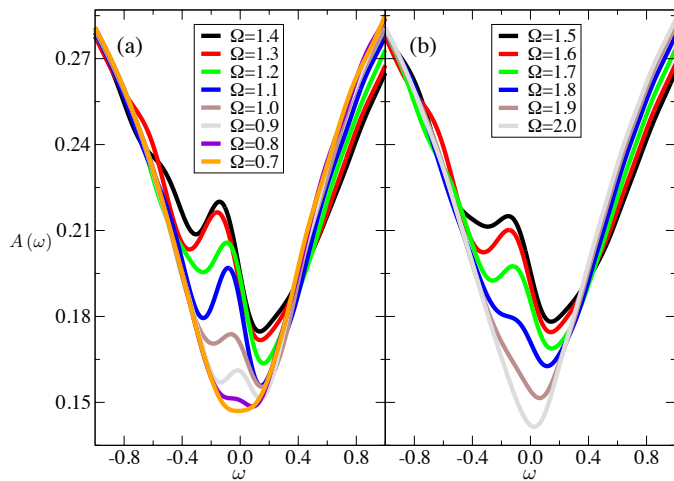


Figure 4. (Color online) Zoom around $\omega \sim 0$ of the time dependent (backward) spectral functions $A(\omega, t) = -\frac{1}{\pi} \text{Im} \int ds G^R(t, t-s) e^{i\omega s}$ at $t = 30$ after excitation pulses with frequency Ω below (a) and above (b) the bare phonon frequency ω_{ph} .

is substituted with (iii) $\langle X(t) \rangle^2$ or (iv) $\langle X^2(t) \rangle$ obtained from the full DMFT calculation. Those approaches lead to

$$U \rightarrow \begin{cases} U - 2(d-h) X^2(t) \equiv U_{X^2}^{\text{s,cl}}(t) \\ U - 2(d-h) \langle X^2(t) \rangle \equiv U_{\langle X^2 \rangle}^{\text{MF}}(t) \\ U - 2(d-h) \langle X(t) \rangle^2 \equiv U_{\langle X \rangle^2}(t) \\ U - 2(d-h) \langle X^2(t) \rangle \equiv U_{\langle X^2 \rangle}(t) \end{cases}, \quad (6)$$

where we have assumed $\sum_i H_i = \sum_i D_i$ up to terms $\propto \dot{N}$. Fig. 2d shows the resulting $U(t)$ for the almost-resonant driving case $\Omega = 1.5$. The two self-consistent protocols are computed using the driving term shown in the inset of Fig. 1. Clearly, for a general state of the quantum phonon, $\langle X \rangle^2 \neq \langle X^2 \rangle$. A time-dependent function of the kind $U(t) = U + \Delta U [1 - \cos(2\omega_{\text{ph}} t)] \theta(t)$ can qualitatively describe the U -driving guided by the classical X or by $\langle X \rangle$, while $U_{\langle X^2 \rangle}(t)$ looks more like an interaction quench. Finally, $U_{\langle X^2 \rangle}^{\text{MF}}(t)$, where the time-dependent $\langle X^2(t) \rangle$ is computed using the density matrix, shows a tiny time-dependence during the action of the external pulse only. Further details about the classical and mean-field dynamics are provided in App. B.

We note that $U_{\langle X^2 \rangle}^{\text{MF}}$ and $U_{\langle X^2 \rangle}$ deviate from U already in equilibrium, where the vacuum and thermal fluctuations of the phonon are responsible for a renormalization of U by ~ -0.3 . In equilibrium, one finds that this renormalization rather accurately accounts for the shift of the IMT in the generalized Hubbard-Holstein model as compared to the standard Hubbard model. In Fig. 1b, we show the equilibrium spectra of the Hubbard model at different U ; the IMT in the Hubbard-Holstein model Eq. (1) is indeed lowered by ~ -0.3 compared to the static one. This quantitative agreement also shows that for the given parameters polaronic effects play a mi-

nor role in localizing the quasi-particles, at least under equilibrium conditions. In contrast to this observation, the non-equilibrium dynamics of quasi-particles and the vibrationally induced IMT in the model cannot be explained by a renormalized time-dependent interaction. We compare in Fig. 3 the time-dependent spectra $A(\omega, t)$ for the full dynamical phonons simulation and the $U_{\langle X^2 \rangle}$ driving protocol, that we take as representative of all the simplified protocols Eq. (6) (indeed, the qualitative dynamics of $A(\omega, t)$ is the same for all of them). While we still notice some increase in the spectral weight at zero frequency, the quench-like $U(t) = U_{\langle X^2 \rangle}(t)$ (lower panels) does not reproduce the emergence of a zero-frequency peak. The rather different response of full DMFT treatment and the simplified approaches (6) is evident also in other observables: the relative change $\Delta d/d \sim 15\%$ in the double occupancy at resonant driving is almost three times larger than the change $\Delta d/d$ in the Hubbard model in response to the corresponding time-dependent interactions (cf. Figs. 2c and e).

A possible explanation of the above findings is that the simplified approaches, which generally replace the phonon operators by semiclassical fields in the electronic problem, have underestimated the phonon-induced dissipation which favors metallization. However, we find that different electronic temperatures cannot explain our results. An effective temperature $1/\beta_{\text{eff}}$ obtained from a fit of the equilibrium fluctuation relation $A^<(\omega, t) = A(\omega, t)/(1 + e^{\beta_{\text{eff}}\omega})$ to the occupation functions $A^<(\omega, t)$ close to $\omega = 0$ at the latest simulation time yields an even lower effective temperature for the $U_{\langle X^2 \rangle}$ -driven case ($\beta_{\text{eff}} \sim 9.5$) compared to the full DMFT results ($\beta_{\text{eff}} \sim 6.2$), see continuous red lines and dotted cyan lines in Figs. 3e and f. Moreover, $1/\beta_{\text{eff}}$ obtained in this way can only characterize the low-energy quasi-particles, while the total energy at $t = 30$ is that of a system at inverse temperature $\beta \sim 2.083$ (spectrum shown by the dashed green line in Fig. 3e), and $\langle X \rangle$ is still oscillating (Fig. 2a). We, therefore, conclude that a time-dependent interaction as in Eq. (6) plus electron cooling cannot faithfully describe the enhancement of metallicity in the photoexcited Mott insulator with nonlinear electron-phonon coupling. An analogous analysis shows that even for states closer to the metal-insulator transition, the enhancement of metallicity is underestimated. A possible explanation is that in addition to the static renormalization of U through $\langle X^2 \rangle$, there is a dynamic contribution via virtual phonon emission and absorption. Such induced interactions go as g^2/ω_{ph} in the anti-adiabatic phonon regime. In the presence of the X^2 -nonlinearity, an oscillating phonon may act similar to a dynamically modulated electron-phonon coupling, which allows for interactions mediated via phonon-Floquet sidebands, with an energy denominator $1/(\omega_{\text{ph}} \pm \Omega)$. Thus, such interactions can be strongly renormalized, in particular close to resonance $\omega_{\text{ph}} = \Omega$. While the present parameter regime, close to the IMT and with not too well-separated energy scales between ω_{ph} and bandwidth,

makes an analytic understanding difficult, the numerical results in Fig. 4 unambiguously demonstrate substantial enhancement of the quasi-particle peak around the resonance. Another effect could be driving-induced undressing of polarons [41–43], but as we have concluded above, polaronic effects are probably not significant here.

Conclusions - In this study, we have analyzed a generalized Hubbard-Holstein model, relevant for the description of molecular solids, which is excited by an ultrafast pulse of local molecular vibration. By exactly treating the quantum phononic fluctuations, we show numerical evidence for the vibrationally-induced emergence of a quasi-particle peak in the electronic spectral function at $\omega \sim 0$, signalling the occurrence of an IMT. This observation should be relevant for the understanding of photo-induced superconductivity in molecular solids [26]. More generally, the striking difference of our results to a simplified treatment for the phonons implies the need for careful analysis of quantum phonon effects in the phononic control of electronic properties.

F.G. would like to thank Nagamalleswararao Dasari for the useful discussions about the Ohmic bath. We were supported by the ERC starting grant No. 716648. The authors gratefully acknowledge the computational resources and support provided by the Erlangen Regional Computing Center (RRZE).

Appendix A: Spectral functions and occupations at intermediate time-steps

In Fig. 3 of the main text, we have shown the time-dependent spectral functions at the initial ($t = 0$) and final ($t = 30$) times of the simulations we performed for the dynamic phonon model and the simplified approach based on the time-dependent Hubbard interaction $U_{\langle X^2 \rangle}(t)$. In the same figure, we have also presented the time evolution of the spectral weight around the Fermi level. Here, we want to show the spectral functions and the respective occupations at intermediate times for the two different cases as depicted in Fig. 5. We notice that the most significant changes of the spectral functions occur around $\omega \sim 0$ and that we observe an overall increase of the spectral weight at the Fermi level in both cases (and, actually, also for the other simplified treatments of the electron-phonon interaction presented in Eq. (6) of the main text). For the dynamic phonon, we recognize the presence of a quasi-particle peak already at $t = 6$. The dynamics of this peak looks pretty interesting: by comparing the snapshots of the spectral function taken at different times, we distinguish the breathing of the peak in both its height and width. The $U_{\langle X^2 \rangle}(t)$ driving leads instead to an almost featureless dynamics, with just a small and featureless increase of the weight at $\omega = 0$ and a slight broadening of the occupation function.

Appendix B: Semiclassical approximation and mean-field decoupling of the electron-phonon interaction

In the main text, we have presented four alternative ways of replacing, in the electron-phonon interaction, the phonon degree of freedom with a classical field or with a simplified treatment of the quantum phonons, see Eq. (6) appearing there. While the two driving protocols of the purely electronic model $U_{\langle X \rangle}(t)$ and $U_{\langle X^2 \rangle}(t)$ do not involve in any sense the phonon part of the Hamiltonian, since the expectation values $\langle X \rangle$ and $\langle X^2 \rangle$ are obtained from the full DMFT calculation, the semiclassical and the mean-field approaches still retain the phonon degree of freedom. In this sense, these last two treatments take into account the back-action of the electrons on the displacement field. The first approach we describe is the semiclassical one, based on the replacement of the quantum operator X_i with a classical and site-independent field X . Similarly, we introduce the classical field P , the conjugate momenta of the generalized coordinate X .

To compute their time evolution, we use the Hamilton equations of motion:

$$\begin{cases} \dot{X}(t) = \omega_{\text{ph}} P(t) \\ \dot{P}(t) = -\frac{\omega_{\text{ph}}^2(d(t))}{\omega_{\text{ph}}} X(t) - \frac{F(t)}{\omega_{\text{ph}}} \end{cases}, \quad (\text{B1})$$

where $\omega_{\text{ph}}^2(d(t)) = \omega_{\text{ph}}^2 \left[1 + \frac{4(h-d)}{\omega_{\text{ph}}} d(t) \right]$, with $d(t) = \frac{1}{N} \sum_i \langle D_i \rangle$ being the time-dependent expectation value of the double occupations. $F(t) = \sqrt{2} \omega_{\text{ph}}^2 f(t)$ is a force field related to external driving. The solution of the system Eq. (B1) provides the time-dependence of the fields $X(t)$ and $P(t)$ so that we can write the time-dependent electronic model that we have to deal with as:

$$H_{\text{U-driv}}(t) = H_{\text{el}} - 2X^2(t)(d-h) \sum_i D_i, \quad (\text{B2})$$

where H_{el} is the electronic part of the original Hamiltonian defined in Eq. (2) of the main text.

This way, we obtain a time-dependent Hubbard interaction written as:

$$U_{X^2}^{\text{s.cl}}(t) = U - 2(d-h)X^2(t). \quad (\text{B3})$$

The Hamiltonian Eq. (B2) corresponds to Eq. (5) in the main text, where the time-dependent Hubbard interaction is provided by Eq. (B3). This equation has to be supplied with Eq. (B1), that provides the time dependence of the field $X(t)$. The dependence of Eq. (B1) by the time-dependent double occupations $d(t)$ leads to a back-action of the electrons on the classical phonon.

By driving the classical field $X(t)$ with an excitation protocol $f(t)$ as depicted in the inset of Fig.1 of the main text, and by using the same Hamiltonian parameters defined there, we obtain the results shown in Fig. 6 (black

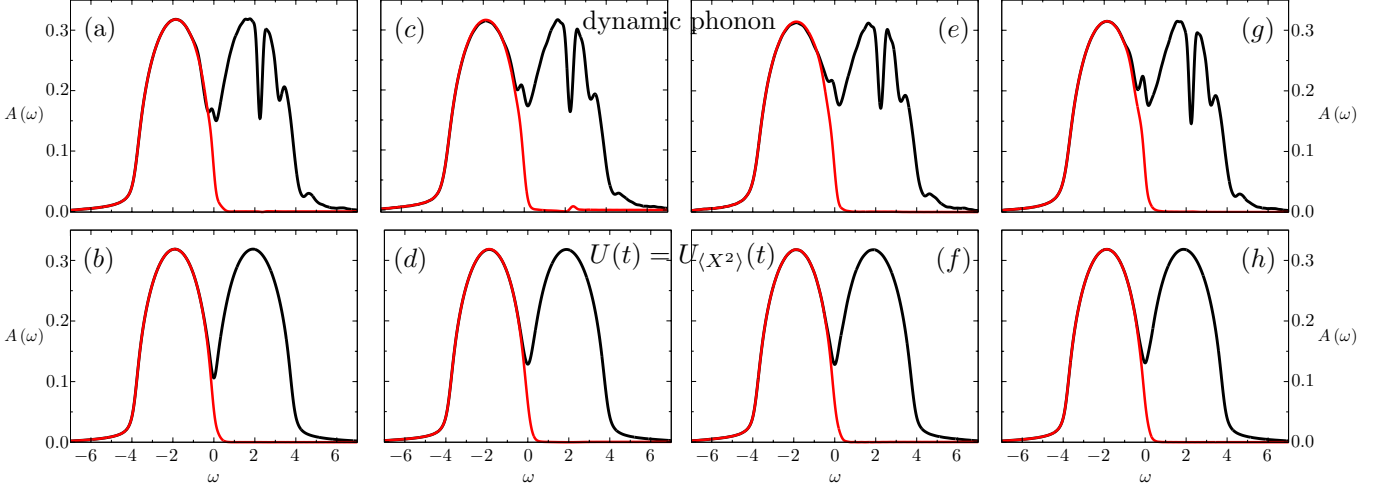


Figure 5. (Color online) Time-dependent spectral functions for the dynamic phonon model at $U = 3.7$ (upper row) and for the simplified model with $U(t) = U_{\langle X^2 \rangle}(t)$ (bottom row) as in Fig. 3 of the main text. Spectral function and occupation (black and red lines, respectively) at time $t = 6$ (panels (a-b)), $t = 12$ (panels (c-d)), $t = 18$ (panels (e-f)) and $t = 24$ (panels (g-h)).

lines). For comparison, we also show the results obtained for the $U_{\langle X^2 \rangle}(t)$ driving already discussed in the main text (red lines).

Fig. 6(a) ((b)) shows the time evolution of $X(t)$ ($P(t)$). The two fields oscillate out of phase at the same frequency close to the bare phonon one ω_{ph} , and they keep doing it even when the pulse is over (we remind that the pulse duration is 20). Fig. 6(c) compares the U -driving experienced by the electronic part of the system during the semiclassical dynamics $U_{X^2}^{\text{s,cl}}(t)$, and for the $U_{\langle X^2 \rangle}(t)$ driving we get from $\langle X(t) \rangle$ obtained with the full DMFT calculation. The comparison between the two gives a qualitative similarity of the results.

Not surprisingly, within the semiclassical phonon treatment, we cannot get two independent renormalizations of the Hubbard interaction as we might get, at the quantum level, from $\langle X \rangle^2$ and $\langle X^2 \rangle$. The reason for this is that, trivially, at the classical level we can simply compute $X^2(t)$ by taking the square of $X(t)$, while this procedure dramatically fails at the quantum level. Thus, to describe a driving protocol based on a field X^2 with an expectation value independent from the one of X , we must rely on a quantum-mechanical description of the operator X^2 . A possible way to keep the quantum nature of the bosonic field is to perform a mean-field decoupling of the electron-phonon interaction presented in Eq. (3) of the main text. This reads:

$$\begin{aligned}
 H_{\text{el-ph}} \rightarrow & 2(h-d)d(t) \sum_i X_i^2 \\
 & + 2(h-d)\langle X^2 \rangle \sum_i D_i \\
 & - 2N(h-d)\langle X^2 \rangle d(t) .
 \end{aligned} \quad (\text{B4})$$

This way, we can separately write the electronic and

phononic mean-field Hamiltonians, coupled one to the other, as:

$$\begin{aligned}
 H_{\text{el}}^{\text{MF}} &= H_{\text{el}} + 2(h-d)\langle X^2(t) \rangle \sum_i D_i , \\
 H_{\text{ph}}^{\text{MF}} &= H_{\text{ph}} + H_{\text{driv}}(t) + 2(h-d)d(t) \sum_i X_i^2 ,
 \end{aligned} \quad (\text{B5})$$

where we omitted the term $-2N(h-d)\langle X^2 \rangle d(t)$ of Eq. (B4).

We solve the electronic part of the model $H_{\text{el}}^{\text{MF}}$ with DMFT at the NCA level. Since the phononic part of the mean-field Hamiltonian is local, we are allowed to write $H_{\text{ph}}^{\text{MF}} = \sum_i H_{\text{ph},i}^{\text{MF}}$. The time evolution of the phonon degree of freedom might thus be computed using the density matrix, that at equilibrium, locally, looks:

$$\rho_{\text{ph},i}^{\text{eq}} = \frac{e^{-\beta H_{\text{ph},i}^{\text{MF}}}}{\text{Tr} [e^{-\beta H_{\text{ph},i}^{\text{MF}}}] } = V \frac{e^{-\beta H_{\text{ph},i,d}^{\text{MF}}}}{\text{Tr} [e^{-\beta H_{\text{ph},i,d}^{\text{MF}}}] } V^\dagger , \quad (\text{B6})$$

where $H_{\text{ph},i}^{\text{MF}} = V_i H_{\text{ph},i,d}^{\text{MF}} V_i^\dagger$ and $H_{\text{ph},i,d}^{\text{MF}}$ is the diagonal form of the local mean-field phononic Hamiltonian $H_{\text{ph},i}^{\text{MF}}$. We underline that, at equilibrium, $H_{\text{driv}}(t)$ is equal to zero. The subsequent time-evolution of the density matrix can be computed via the Von Neumann equation:

$$\frac{\partial \rho_{\text{ph},i}(t)}{\partial t} = -i [H_{\text{ph},i}^{\text{MF}}, \rho_{\text{ph},i}(t)] , \quad (\text{B7})$$

with initial condition provided by $\rho_{\text{ph},i}(t=0) = \rho_{\text{ph},i}^{\text{eq}}$.

A convenient basis for expressing the density matrix, as well as $H_{\text{ph}}^{\text{MF}}$, is the one of the local phonon Fock space so that we can write:

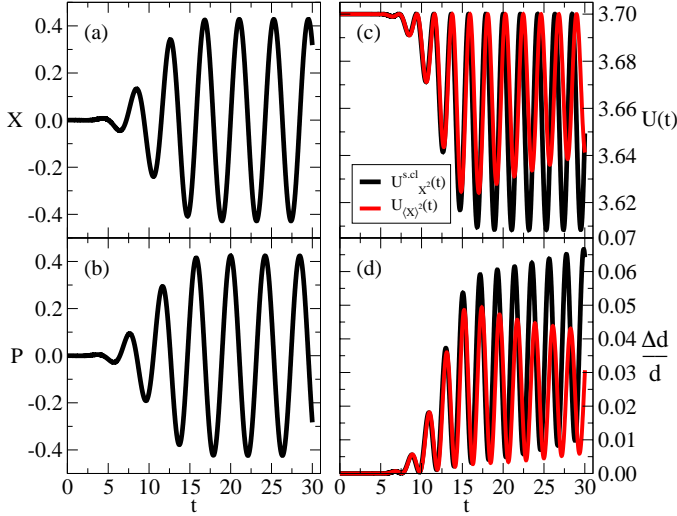


Figure 6. Time evolution of the classical fields $X(t)$ and $P(t)$ (panels (a) and (b), respectively) and the corresponding changes in the Hubbard interaction $U_{X^2}^{s,cl}(t)$ and in the relative change in the double occupations $\Delta d/d$ (panels (c) and (d), respectively) for the same excitation protocol shown in the inset of Fig. 1 of the main text (black lines). For comparison, in panels (c) and (d) we show the results for the time dependent protocol $U_{\langle X^2 \rangle}(t)$ (red lines). The lines in panels (c) and (d) are already shown in Fig. 2(d) and (e) of the main text.

$$\begin{aligned}
 (H_{\text{ph},i})_{n,p} &= \omega_{\text{ph}} N \left(p + \frac{1}{2} \right) \delta_{n,p}, \\
 (H_{\text{driv},i}(t))_{n,p} &= \omega_{\text{ph}} N f(t) \left[\sqrt{p+1} \delta_{n,p+1} + \sqrt{p} \delta_{n,p-1} \right], \\
 2N(h-d)d(t)(X_i^2)_{n,p} &= N(h-d)d(t) \\
 & \left[\sqrt{p(p-1)} \delta_{n,p-2} + (1+2p) \delta_{n,p} \right. \\
 & \left. + \sqrt{(p+1)(p+2)} \delta_{n,p+2} \right].
 \end{aligned} \tag{B8}$$

From the knowledge of the time-dependent density matrix $\rho_{\text{ph},i}(t)$, we compute the time-dependent expectation value of X_i^2 as:

$$\langle X^2(t) \rangle = \text{Tr} [\rho_{\text{ph},i}(t) X_i^2]. \tag{B9}$$

Given this quantity, we can also compute:

$$U_{\langle X^2 \rangle}^{\text{MF}}(t) = U - 2(d-h) \langle X^2(t) \rangle, \tag{B10}$$

defined in Eq. (6) of the main text.

In Fig. 7, we show the results obtained at the mean-field level by considering the quantum phonons in the presence of an external driving equal to the one shown

in the inset of Fig. 1 of the main text. We notice that $\langle X^2(t) \rangle = \langle X(t) \rangle^2 + \langle X^2(0) \rangle$, where $\langle X^2(0) \rangle \sim 0.5082$. The time dependence of $\langle X(t) \rangle$ and of $\langle X^2(t) \rangle$, shown

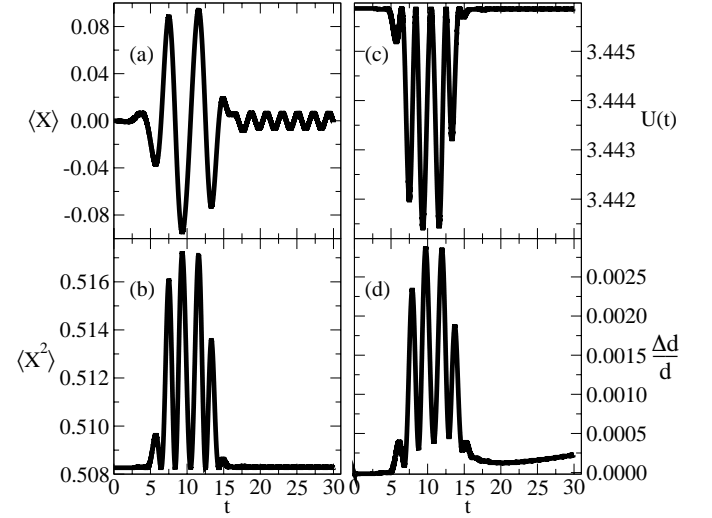


Figure 7. Time evolution of the expectation values $\langle X(t) \rangle$ and $\langle X^2(t) \rangle$ (panels (a) and (b), respectively) and the corresponding changes in the Hubbard interaction $U_{\langle X^2 \rangle}^{\text{MF}}(t)$ and in the relative change in the double occupations $\Delta d/d$ (panels (c) and (d), respectively) for the same excitation protocol shown in the inset of Fig. 1 of the main text. We stress that the curves in panels (c) and (d) are shown also in Fig. 2(d) and (e) of the main text, respectively.

in Fig. 7(a) and (b), respectively, does not resemble the one presented in the main text in panels (a) and (b) of Fig. 2 (black lines) and neither the one shown in Fig. 6(a) for the classical field X . Indeed, in this mean-field calculation, we observe that the oscillatory behavior of both $\langle X(t) \rangle$ and $\langle X^2(t) \rangle$ is the most pronounced while the external pulse is active. Instead, when the external perturbation is over, the response of the system is strongly suppressed. The frequency of the oscillations observed in $\langle X(t) \rangle$ for $t > 20$ is almost equal to the double of the bare phonon frequency $2 \times \omega_{\text{ph}}$. This fact, together with the small response of the system for a driving frequency $\Omega = \omega_{\text{ph}}$, are in qualitative agreement with the picture provided by the parametric oscillator. The quench in $\langle X^2(t) \rangle$ after the pulse observed in the full NCA calculation here disappears. Also, the relative change in the double occupations in Fig. 7(d) is different as compared to the one presented in Fig. 2(c) of the manuscript (black line) both from the quantitative and the qualitative point of view.

To briefly summarize our findings, we observe that the simplified protocol $U_{\langle X^2 \rangle}(t)$ introduced in the main text (violet line in Fig. 2(d)) produces a $\Delta d/d$ that compares much better to the NCA result with respect to the ones obtained with all the other simplified U -drivings introduced in Eq. (6) of the main text.

- [1] M. Först, C. Manzoni, S. Kaiser, Y. Tomioka, Y. Tokura, R. Merlin, and A. Cavalleri, “Nonlinear phononics as an ultrafast route to lattice control,” *Nature Physics* **7**, 854–856 (2011).
- [2] Alaska Subedi, Andrea Cavalleri, and Antoine Georges, “Theory of nonlinear phononics for coherent light control of solids,” *Phys. Rev. B* **89**, 220301(R) (2014).
- [3] D. N. Basov, R. D. Averitt, and D. Hsieh, “Towards properties on demand in quantum materials,” *Nature Materials* **16**, 1077–1088 (2017).
- [4] Matteo Rini, Ra’anan Tobey, Nicky Dean, Jiro Itatani, Yasuhide Tomioka, Yoshinori Tokura, Robert W Schoenlein, and Andrea Cavalleri, “Control of the electronic phase of a manganite by mode-selective vibrational excitation,” *Nature* **449**, 72–74 (2007).
- [5] A. D. Caviglia, R. Scherwitzl, P. Popovich, W. Hu, H. Bromberger, R. Singla, M. Mitrano, M. C. Hoffmann, S. Kaiser, P. Zubko, S. Gariglio, J.-M. Triscone, M. Först, and A. Cavalleri, “Ultrafast strain engineering in complex oxide heterostructures,” *Phys. Rev. Lett.* **108**, 136801 (2012).
- [6] R. Mankowsky, A. Subedi, M. Först, S. O. Mariager, M. Chollet, H. T. Lemke, J. S. Robinson, J. M. Glowina, M. P. Minitti, A. Frano, M. Fechner, N. A. Spaldin, T. Loew, B. Keimer, A. Georges, and A. Cavalleri, “Nonlinear lattice dynamics as a basis for enhanced superconductivity in $\text{YBa}_2\text{Cu}_3\text{O}_{6.5}$,” *Nature* **7529**, 71–73 (2014).
- [7] M. Först, R. I. Tobey, S. Wall, H. Bromberger, V. Khanna, A. L. Cavalieri, Y.-D. Chuang, W. S. Lee, R. Moore, W. F. Schlotter, J. J. Turner, O. Krupin, M. Trigo, H. Zheng, J. F. Mitchell, S. S. Dhesi, J. P. Hill, and A. Cavalleri, “Driving magnetic order in a manganite by ultrafast lattice excitation,” *Phys. Rev. B* **84**, 241104(R) (2011).
- [8] M. Först, A. D. Caviglia, R. Scherwitzl, R. Mankowsky, P. Zubko, V. Khanna, H. Bromberger, S. B. Wilkins, Y.-D. Chuang, W. S. Lee, W. F. Schlotter, J. J. Turner, G. L. Dakovski, M. P. Minitti, J. Robinson, S. R. Clark, D. Jaksch, J.-M. Triscone, J. P. Hill, S. S. Dhesi, and A. Cavalleri, “Spatially resolved ultrafast magnetic dynamics initiated at a complex oxide heterointerface,” *Nature Materials* **14**, 883–888 (2015).
- [9] T. F. Nova, A. Cartella, A. Cantaluppi, M. Först, D. Bossini, R. V. Mikhaylovskiy, A. V. Kimel, R. Merlin, and A. Cavalleri, “An effective magnetic field from optically driven phonons,” *Nature Physics* **2**, 132–136 (2017).
- [10] E. Pomarico, M. Mitrano, H. Bromberger, M. A. Sentef, A. Al-Temimy, C. Coletti, A. Stöhr, S. Link, U. Starke, C. Cacho, R. Chapman, E. Springate, A. Cavalleri, and I. Gierz, “Enhanced electron-phonon coupling in graphene with periodically distorted lattice,” *Phys. Rev. B* **95**, 024304 (2017).
- [11] R. Singla, G. Cotugno, S. Kaiser, M. Först, M. Mitrano, H. Y. Liu, A. Cartella, C. Manzoni, H. Okamoto, T. Hasegawa, S. R. Clark, D. Jaksch, and A. Cavalleri, “Thz-frequency modulation of the hubbard u in an organic mott insulator,” *Phys. Rev. Lett.* **115**, 187401 (2015).
- [12] Dante M. Kennes, Eli Y. Wilner, David R. Reichman, and Andrew J. Millis, “Transient superconductivity from electronic squeezing of optically pumped phonons,” *Nature Physics* **13**, 479–483 (2017).
- [13] M. A. Sentef, “Light-enhanced electron-phonon coupling from nonlinear electron-phonon coupling,” *Phys. Rev. B* **95**, 205111 (2017).
- [14] Alexandre Marciniak, Stefano Marcantoni, Francesca Giusti, Filippo Glerean, Giorgia Sparapassi, Tobia Nova, Andrea Cartella, Simone Latini, Francesco Valiera, Angel Rubio, Jeroen van den Brink, Fabio Benatti, and Daniele Fausti, “Vibrational coherent control of localized d-d electronic excitation,” arXiv e-prints, arXiv:2003.13447 (2020), arXiv:2003.13447 [cond-mat.mtrl-sci].
- [15] M. Puviani and M. A. Sentef, “Quantum nonlinear phononics route towards nonequilibrium materials engineering: Melting dynamics of a ferroelectric charge density wave,” *Phys. Rev. B* **98**, 165138 (2018).
- [16] Avraham Klein, Morten H. Christensen, and Rafael M. Fernandes, “Laser-induced control of an electronic nematic quantum phase transition,” *Phys. Rev. Research* **2**, 013336 (2020).
- [17] Michael Lang and Jens Müller, “Organic superconductors,” in *The Physics of Superconductors: Vol. II. Superconductivity in Nanostructures, High-Tc and Novel Superconductors, Organic Superconductors*, edited by K. H. Bennemann and J. B. Ketterson (Springer Berlin Heidelberg, Berlin, Heidelberg, 2004) pp. 453–554.
- [18] Arzhang Ardavan, Stuart Brown, Seiichi Kagoshima, Kazushi Kanoda, Kazuhiko Kuroki, Hatsumi Mori, Masao Ogata, Shinya Uji, and Jochen Wosnitza, “Recent topics of organic superconductors,” *Journal of the Physical Society of Japan* **81**, 011004 (2012).
- [19] H. Okamoto, H. Matsuzaki, T. Wakabayashi, Y. Takahashi, and T. Hasegawa, “Photoinduced metallic state mediated by spin-charge separation in a one-dimensional organic mott insulator,” *Phys. Rev. Lett.* **98**, 037401 (2007).
- [20] M. Mitrano, G. Cotugno, S. R. Clark, R. Singla, S. Kaiser, J. Stähler, R. Beyer, M. Dressel, L. Baldassarre, D. Nicoletti, A. Perucchi, T. Hasegawa, H. Okamoto, D. Jaksch, and A. Cavalleri, “Pressure-dependent relaxation in the photoexcited mott insulator $\text{ET-F}_2\text{TCNQ}$: Influence of hopping and correlations on quasiparticle recombination rates,” *Phys. Rev. Lett.* **112**, 117801 (2014).
- [21] S. Kaiser, S. R. Clark, D. Nicoletti, G. Cotugno, R. I. Tobey, N. Dean, S. Lupi, H. Okamoto, T. Hasegawa, D. Jaksch, and A. Cavalleri, “Optical properties of a vibrationally modulated solid state mott insulator,” *Scientific Reports* **4**, 3823 (2014).
- [22] Massimo Capone, Michele Fabrizio, Claudio Castellani, and Erio Tosatti, “Colloquium: Modeling the unconventional superconducting properties of expanded A_3C_{60} fullerides,” *Rev. Mod. Phys.* **81**, 943–958 (2009).
- [23] M. Mitrano, A. Cantaluppi, D. Nicoletti, S. Kaiser, A. Perucchi, S. Lupi, P. Di Pietro, D. Pontiroli, M. Riccò, S. R. Clark, D. Jaksch, and A. Cavalleri, “Possible light-induced superconductivity in k_3C_{60} at high temperature,” *Nature* **7591**, 461–464 (2016).
- [24] A. Cantaluppi, M. Buzzi, G. Jotzu, D. Nicoletti, M. Mitrano, D. Pontiroli, M. Riccò, A. Perucchi, P. Di Pietro, and A. Cavalleri, “Pressure tuning of light-induced superconductivity in k_3C_{60} ,” *Nature Physics* **8**, 837–841 (2018).

- [25] M. Budden, T. Gebert, M. Buzzi, G. Jotzu, E. Wang, T. Matsuyama, G. Meier, Y. Laplace, D. Pontiroli, M. Riccò, F. Schlawin, D. Jaksch, and A. Cavalleri, “Evidence for metastable photo-induced superconductivity in K_3C_{60} ,” arXiv e-prints, arXiv:2002.12835 (2020), arXiv:2002.12835 [cond-mat.supr-con].
- [26] M. Buzzi, D. Nicoletti, M. Fechner, N. Tancogne-Dejean, M. A. Sentef, A. Georges, T. Biesner, E. Uykur, M. Dressel, A. Henderson, T. Siegrist, J. A. Schlueter, K. Miyagawa, K. Kanoda, M.-S. Nam, A. Ardavan, J. Coulthard, J. Tindall, F. Schlawin, D. Jaksch, and A. Cavalleri, “Photomolecular high-temperature superconductivity,” *Phys. Rev. X* **10**, 031028 (2020).
- [27] Y. Kawakami, S. Iwai, T. Fukatsu, M. Miura, N. Yoneyama, T. Sasaki, and N. Kobayashi, “Optical modulation of effective on-site coulomb energy for the mott transition in an organic dimer insulator,” *Phys. Rev. Lett.* **103**, 066403 (2009).
- [28] P. Pincus, “Polaron effects in the nearly atomic limit of the hubbard model,” *Solid State Communications* **11**, 51–54 (1972).
- [29] J. E. Hirsch, “Dynamic hubbard model,” *Phys. Rev. Lett.* **87**, 206402 (2001).
- [30] K. Itoh, H. Itoh, M. Naka, S. Saito, I. Hosako, N. Yoneyama, S. Ishihara, T. Sasaki, and S. Iwai, “Collective excitation of an electric dipole on a molecular dimer in an organic dimer-mott insulator,” *Phys. Rev. Lett.* **110**, 106401 (2013).
- [31] Daniel Neuhauser, Tae-Jun Park, and Jeffrey I. Zink, “Analytical derivation of interference dips in molecular absorption spectra: Molecular properties and relationships to fano’s antiresonance,” *Phys. Rev. Lett.* **85**, 5304–5307 (2000).
- [32] J. E. Hirsch, “Electron-hole asymmetry is the key to superconductivity,” *International Journal of Modern Physics B* **17**, 3236–3241 (2003).
- [33] Hideo Aoki, Naoto Tsuji, Martin Eckstein, Marcus Kollar, Takashi Oka, and Philipp Werner, “Nonequilibrium dynamical mean-field theory and its applications,” *Reviews of Modern Physics* **86**, 779–837 (2014).
- [34] Martin Eckstein and Philipp Werner, “Nonequilibrium dynamical mean-field calculations based on the noncrossing approximation and its generalizations,” *Phys. Rev. B* **82**, 115115 (2010).
- [35] Hugo U. R. Strand, Martin Eckstein, and Philipp Werner, “Nonequilibrium dynamical mean-field theory for bosonic lattice models,” *Phys. Rev. X* **5**, 011038 (2015).
- [36] Philipp Werner and Martin Eckstein, “Phonon-enhanced relaxation and excitation in the holstein-hubbard model,” *Phys. Rev. B* **88**, 165108 (2013).
- [37] Philipp Werner and Martin Eckstein, “Effective doublon and hole temperatures in the photo-doped dynamic hubbard model,” *Structural Dynamics* **3**, 023603 (2016).
- [38] Hsing-Ta Chen, Guy Cohen, Andrew J. Millis, and David R. Reichman, “Anderson-holstein model in two flavors of the noncrossing approximation,” *Phys. Rev. B* **93**, 174309 (2016).
- [39] Martin Eckstein and Philipp Werner, “Photoinduced States in a Mott Insulator,” *Physical Review Letters* **110**, 126401 (2013).
- [40] Francesco Peronaci, Olivier Parcollet, and Marco Schiró, “Enhancement of local pairing correlations in periodically driven mott insulators,” *Phys. Rev. B* **101**, 161101(R) (2020).
- [41] J. E. Hirsch, “Quasiparticle undressing in a dynamic hubbard model: Exact diagonalization study,” *Phys. Rev. B* **66**, 064507 (2002).
- [42] J. E. Hirsch, “Polaronic superconductivity in the absence of electron-hole symmetry,” *Phys. Rev. B* **47**, 5351–5358 (1993).
- [43] P. Gaal, W. Kuehn, K. Reimann, M. Woerner, T. Elsaesser, and R. Hey, “Internal motions of a quasiparticle governing its ultrafast nonlinear response,” *Nature* **450**, 1210–1213 (2007).